THE PERFORMANCE OF ACCELEROMETERS, MICROPHONES AND PVDF SENSORS IN ACTIVE STRUCTURAL ACOUSTIC CONTROL: THEORETICAL ANALYSIS

Bor-Tsuen Wang *
Department of Mechanical Engineering
National Pingtung Polytechnic Institute
Pingtung, Taiwan 91207, R.O.C.

Abstract- *This paper analytically demonstrates the performance of accelerometers, microphones and PVDF sensors in active structural sound radiation control. A harmonic point force disturbance applied to a simply-supported beam mounted with an infinite rigid baffle is considered as the primary source. The piezoelectric actuators bonded to the beam surface are used as secondary sources to attenuate the sound radiation through the beam. Different types of error sensors are used to perform active coutrol to reduce sound radiation level. An optimal process is applied to obtain the input voltages of piezoelectric actuators so that the cost funciton can be minimized. The cost function which is the least mean square value of the sensor signal is constructed based on the type of error sensor. Results show that a reduction of sound radiation through the beam can be successfully achieved, if the proper type, number and position of sensors and actuators are selected. Additionally, a comparison shows that microphones provide more effective control of sound radiation than accelerometers and PVDF sensors; however, PVDF sensors have practical advantages over accelerometers and microphones because of their low cost and light weight.*

Keywords:acceleroneter, microphone, PVDF, sound radation, control

INTRODUCTION

Active structural acoustic control (ASAC) has been drawn a great deal of interest over the past few years. Upon the development of fast processing micro-chips, many pc-based control algorithms have been developed and successfully applied to ASAC [1-3]. Leug [4] first proposed to cancel a sound field by superimposing a secondary sound source of opposite phase. Although the sound source is not a "real" actuator, many applications have been shown that the use of sound sources can effectively attenuate the radiated sound pressure level [5,6]. Another effective mean to control the structural sound radiation is to apply control force directly to the radiated structure. Shakers are frequently used as control forces [7,8]. Recently, the distributed types of actuators, such as piezoelectric actuators, have been shown the feasible implementation and sufficient control in ASAC [9,10].

The selection of error sensors is also a key factor to perform effective ASAC. Microphones are generally used as error sensors in ASAC; however, that microphones must be located in the radiated far-field makes them impractical for applications. Structural sensors, such as accelerometers, have been proposed for ASAC [3]. Although accelerometers overcome the disadvantages of far-field sensors, accelerometers are still impractical for implementation due to the high cost and the difficulty to adhere to the structure. PVDF sensor which is a film type of sensor attached to the structure has been applied to structural vibration and acoustic control [11,12]. The PVDF sensors are more practical than microphones or accelerometers for applications because of their compactness and low cost.

This work studies the sound radiation control of a simply-supported beam with infinite baffle. A harmonically excited point force acting on the beam is assumed to be the primary source (disturbance), while the piezoelectric actuator is applied as the secondary source (control force) to reduce the motion of the structural field as well as the acoustic field. Different forms of sensing devices, such as accelerometers, microphones and PVDF films, are used as the error sensors. They may be either located on the near-field structure or in

* Associate Professor

the radiated far-field. A minimization process which is to simulate the LMS feedforward control algorithm is performed to obtain the control voltages applied to the actuator so as to minimize the cost function. The cost function is the least mean square value of the sensor signals and can be constructed based on the types of error sensors applied. The radiation directivity pattern are studied to show the control effectiveness as well as the wavenumber analysis. Results show that sufficient control can be achieved, if the proper sensors and actuators are used. A comparison is also shown that microphones provide more effective control of sound radiation than accelerometers and PVDF sensors; however PVDF sensors are more practical than accelerometers and microphones because of their low cost and light weight. This work also lays out the idea for the design of active noise control system.

2.THEORETICAL ANALYSIS

2.1 Lateral Vibration of Uniform Beam

Consider a uniform simply-supported beam with length of L, as shown in Figure 1, the equation of motion can be obtained as follow:

$$E_b I\frac{\partial^4 w}{\partial x^4}+\rho_b b t_b\frac{\partial^2 w}{\partial t^2}=p(x,t) \tag{1}$$

where E_b is the Young's modulus of the beam; I the moment of inertia; ρ_b the beam density; t_b the beam thickness; b the beam width; $p(x,t)$ the force function. Note that the damping effect is assumed small and can be neglected for simple application. The boundary condition for a simply- supported beam are

$$M(0,t)=M(L,t)=E_b I\frac{\partial^2 w}{\partial x^2}=0 \tag{2}$$

$$w(0,t)=w(L,t)=0 \tag{3}$$

For free vibration analysis, i.e., $p(x,t)=0$, the natural frequencies can be found to be

$$\omega_n=(n\pi)^2\sqrt{\frac{E_b I}{\rho_b b t_b L^4}} \tag{4}$$

The general form of beam lateral displacement, while the beam is subjected to harmonic force inputs, can be written as the follow:

$$w(x,t)=e^{i\omega t}\sum_{n=1}^{\infty}W_n\sin\alpha_n x \tag{5}$$

where

$$\alpha_n=\frac{n\pi}{L} \tag{6}$$

$$W_n=\frac{P_n}{\rho_b b t_b(\omega_n^2-\omega^2)} \tag{7}$$

Here ω is the excitation frequency; α_n is the modal number; W_n is the modal amplitude; and P_n is the modal force depending on the forms of external forces. For a harmonic point force with the amplitude of F located at x_f acting on the beam, the force function, p(x,t) can be written as follow:

$$p(x,t)=F\delta(x-x_f)e^{i\omega t} \tag{8}$$

The Delta function, $\delta(x)$, is employed to represent the location of the point force. The modal force, P_n^f, due to the point force excitation is given as follow:

$$P_n^f=\frac{2F}{L}\sin\alpha_n x_f \tag{9}$$

where the superscript f signify the point force. For an actuator consisting of two identical piezoceramic patches bonded symmetrically on the two opposite beam surfaces and activated 180° out-of-phase, the equivalent external forces can be derived as follow [13]:

$$p(x,t)=M_{eq}[\delta'(x-x_1)-\delta'(x-x_2)]e^{i\omega t} \tag{10}$$

where M_{eq} is the concentrated moments acting on the both edges of piezoelectric patches represented by the first derivative of Delta function. The corresponding expression of modal force for piezoelectric excitation, P_n^c, can be derived [13] as follow:

$$P_n^c=\frac{2M_{eq}}{L}\alpha_n(\cos\alpha_n x_1-\cos\alpha_n x_2) \tag{11}$$

where x_1 and x_2 are the coordinates of the piezoelectric actuator, and the superscript c signify the control force.

PVDF sensors' equations

For a PVDF film arranged as shown in Figure 1, the shape function can be expressed as follow:

$$\Gamma(x)=u(x-x_{s1})-u(x-x_{s2}) \tag{12}$$

where $u(x)$ is the step function; x_{s1} and x_{s2} are the coordinates of the PVDF film. The sensor's equation can then be derived as follows [14]:

$$q(t)=\frac{t_b+t_s}{2}b_s e_{31}\int_0^L\Gamma(x)\frac{\partial^2 y}{\partial x^2}dx \tag{13}$$

where b_s is the sensor width; t_s the sensor thickness; e_{31} the piezoelectric field intensity constant. By substituting $w(x,t)$ and integrating over the beam length,

$$q(t)=e^{i\omega t}\left(\frac{t_b+t_s}{2}e_{31}b\right)\sum_{n=1}^{\infty}\alpha_n W_n(\cos\alpha_n x_{s2}-\cos\alpha_n x_{s1}) \tag{14}$$

The generated voltages can then be expressed as:

$$V(t)=\frac{q(t)}{\epsilon A}t_s \tag{15}$$

where ϵ is the permittivity of PVDF films; A is the sensor area. It is noted that the generated voltage is proportional to the slope difference between the two edges of a PVDF film.

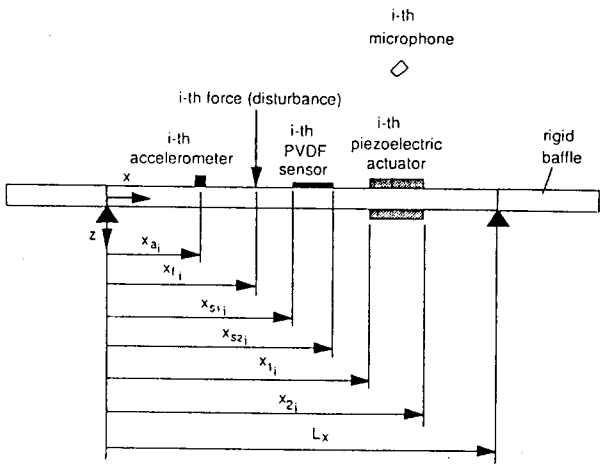

Fig.1 The Arrangement and Coordinates of Baffled Simply-Supported Beam

2.2 Sound Radiated in the Far-Field

The far-field sound pressure radiated from a vibrating surface at a point in the acoustic field, as shown in Figure 2, is given by the Rayleigh integral [15]:

$$p(\vec{r},t) = \frac{i\omega\rho}{2\pi}\int_s \dot{w}(\vec{r}_s)\frac{e^{-ikR}}{R}ds \qquad (16)$$

where $\vec{r}$ is the position vector of the observation point; $\vec{r}_s$ is the position vector of the elemental surface ds; $\dot{w}(\vec{r}_s)$ is the normal velocity of ds; R is $|\vec{r}-\vec{r}_s|$; ρ is the fluid density; and $k=\omega/c$ is the acoustic wavenumber. Here, the acoustic medium is air, and thus there is no feedback of the fluid motion into the structure. By substituting the beam velocity derived from Equation (5) into the Rayleigh integral, the sound pressure radiated to the far-field can be obtained [16]:

$$p(r,\theta,\phi,t) = e^{i\omega t}\sum_{n=1}^{\infty} W_n q_n \qquad (17)$$

where

$$q_n = i\omega\frac{\rho c b}{\pi}\frac{k}{\alpha_n}\frac{e^{-ikr}}{2r}\left[\frac{1-(-1)^n e^{-i\alpha}}{1+(\alpha/n\pi)^2}\right]\left[\frac{1-e^{-i\beta}}{\beta}\right] \qquad (18)$$

$$\alpha = kL\sin\theta\cos\phi \qquad (19)$$

$$\beta = kb\sin\theta\sin\phi \qquad (20)$$

Under the assumption of superposition, the total radiated sound pressure can be the sum of sound pressures due to the disturbance and control imputs

$$p_t = p_f + p_c = e^{i\omega t}\sum_{n=1}^{\infty}(W_n^f + W_n^c)q_n \qquad (21)$$

The total radiated sound power defined as the integral of the square of the radiated sound pressure over the hemisphere of the radiating field can then be obtained:

$$\Phi_p = \frac{1}{2\rho c}\int_s |p_t|^2 dS = \frac{r^2}{2\rho c}\int_0^{2\pi}\int_0^{\pi/2}|p_t|^2\sin\theta d\theta d\phi \qquad (22)$$

The total radiated sound power can be an index to evaluate the effectiveness of sound radiation control.

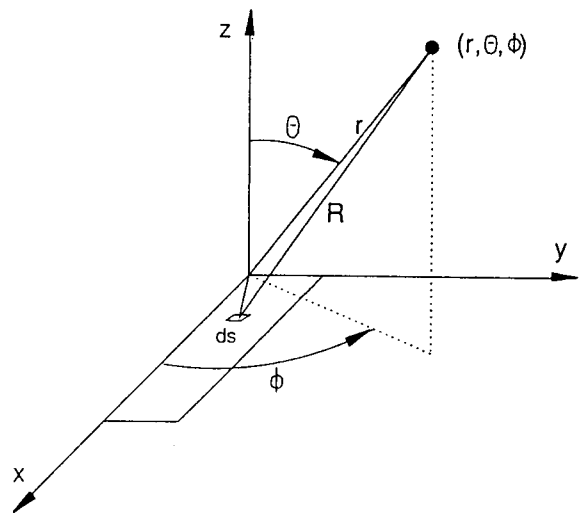

Fig.2 Sound Radiated Coordinates System

2.3 Wavenumber Analysis

The beam velocity distribution can be taken Fourier integral transform in k-plane.

$$\tilde{V}(k_x,k_y) = \int_{-\infty}^{\infty}\int_{-\infty}^{\infty}\dot{w}(x)e^{-i(k_x x+k_y y)}dxdy \qquad (23)$$

where

$$k_x = k\sin\theta\cos\phi \qquad (24)$$

$$k_y = k\sin\theta\sin\phi \qquad (25)$$

therefore, the velocity transform can be expressed as:

$$\tilde{V}(k_x,k_y) = i\omega\sum_{n=1}^{\infty} W_n V_n \qquad (26)$$

where

$$V_n = i\alpha_n\left[\frac{1-(-1)^n e^{-ik_x L}}{\alpha_n^2-k_x^2}\right]\left[\frac{e^{-ik_y b}-1}{k_y}\right] \qquad (27)$$

It is noted that the least mean square (LMS) value of the velocity transform, i.e., $|\tilde{V}|^2$, is proportional to the radiated sound power [15]. Only the wavenumber components satisfying $k_x^2+k_y^2 < k^2$ contribute to sound radiation into the far-field and are termed as supersonic waves. Other wavenumber components do not radiate into the far-field and are termed subsonic waves.

2.4 Cost Functions

For the use of N_a accelerometers, the cost function can be defined as the sum of the mean square of measured accelerations:

$$\Psi_a = \sum_{j=1}^{N_a} |\ddot{w}(x_{aj})|^2 \tag{28}$$

For the use of N_m microphones, the cost function can be defined as the sum of the mean square of measured sound pressure:

$$\Psi_p = \sum_{j=1}^{N_m} |p_t(r_j, \theta_j, \phi_j)|^2 \tag{29}$$

For the use of N_s PVDF sensors, the cost function can be defined as the sum of the mean square voltages measured from the PVDF films:

$$\Psi_v = \sum_{j=1}^{N_s} |V_j|^2 \tag{30}$$

The linear quadratic optimal control theory (LQOCT) can then be applied to minimize the cost function so as to find the optimal control voltages input to the piezoelectric actuators. Either one of the cost functions mentioned above is obviously quadratic and positive definite and possesses a unique minimum. One can easily perform a minimization procedures [1] to calculate the optimal control parameters so as to minimize the cost function. The full analysis can be referred to [17] and omitted here for brevity. The vibrating energy of the beam can be expressed as follow:

$$\Phi_w = \int_0^L |\ddot{w}|^2 dx \tag{31}$$

which can used as an index to evaluate the effectiveness of vibration control.

3.NUMERICAL RESULTS AND DISCUSSIONS

A steel beam with length of 0.38m, width of 0.04m, and thickness of 2mm is used in the simulations. The first few natural frequencies are 33.2Hz, 128.8Hz, 289.9Hz, 515.4Hz, 805.3Hz and 1159.6Hz. It is noted that no damping was included in the following analysis. The optimal process is suitable for controlling multiple primary sources; however, only one harmonic point force with input parameters, F=0.1N and $x_f = 0.067m$, was considered for the following analysis. The piezoelectric patch (G-1195) [18] and PVDF films (LDT-28μ k) [19] are respectively used. The piezoceramic patch is located at $x_1 = 0.285m, x_2 = 0.3485m$.

For comparing the control performance of accelerometers, microphones and PVDF sensors, three locations of each sensor are selected. A1 ($x_a = 0.095m$), A2 ($x_a = 0.19m$) and A3 ($x_a = 0.285m$) represent the accelerometers, M1 ($r, \theta, \phi = 1m, 45°, 0°$), M2 ($r, \theta, \phi = 1m, 0°, 0°$) and M3 (r, $\theta, \phi = 1m, 45°, 180°$) the microphones, and P1 ($x_{s1} = 0.075m, x_{s2} = 0.115m$), P2 ($x_{s1} = 0.17m, x_{s2} = 0.21m$) and P3 ($x_{s1} = 0.265m, x_{s2} = 0.305m$) the PVDF sensors. The accelerometers are located at about one third of the beam length, i.e., near the maximum response of the third modal response. The central location of each PVDF sensor is corresponding to the accelerometer's location. All of the PVDF films have the length of 0.04m. The microphones are arranged at the circle with the radius of 1m above the beam. Each microphones is 45° apart from each other as shown in Figure 3(b). The location of microphones is approximately corresponding to the maximum sound pressure of the third radiation mode. Both on-and off-resonance excitation cases are presented and compared for the control performance of the three types of sensors in terms of radiation directivity pattern, wavenumber analysis and beam displacement response.

It order to calculate the beam response and radiated sound pressure, it was necessary to truncate the modal sums in Equation (5). Upon consideration of computing time and accuracy, the first 10 modes were considered, and it was found to provide sufficient convergence of series. Both the radiation directivity and beam displacement distributions were shown to demonstrate the control effectiveness of sound radiation through the beam. The radiated sound pressure is plotted in dB re 20×10^{-6} Pa over $\theta = -90°$ to 90°, while the beam displacement distribution is normalized by the largest amplitude in each case and plotted in dB along the beam length.

3.1 On-resonance case

Figure 3 shows the radiation directivity for on-resonance excitation near the third mode. On the top of each plot, the arrangement of actuators and sensors is depicted. The solid line indicates the sound pressure level due to the disturbance alone. That the radiation mode shape reveals a non-uniform monopole response evidences the existence of the third mode. With applying control, a global reduction of sound pressure level can be achieved leaving different residual directivity patterns for the use of different types and location of sensors. The residual radiation mode shapes are similar for the cases of using accelerometers and PVDF films, i.e., known as the near-field structural sensors. As shown in Figure 3(b) for the use of microphones, the residual radiation mode shape reveals a dip at the microphone location due to the minimization of the cost function. Table 1 summarizes the results for on-resonance cases. One can observe that the M2 microphone provides the most reduction of radiated power

59 dB, while the A2 accelerometer provides the most reduction of vibrating energy 55 dB. With the proper selection of location of sensors, a global reduction of sound pressure can be observed. In particular, the use of microphones achieves better sound radiation control than accelerometers and PVDF films, because microphones directly measure the acoustic field, while accelerometers and PVDF films measure the structural field. Conversely, in term of the reduction of vibrating energy, accelerometers are more effective than others. For the use of PVDF film sensors, sufficient control can be achieved. It is noted that the distributed type of PVDF film sensors can overcome the disadvantages of accelerometers and microphones as mentioned in Introduction and are more practical for applications.

Table 1 Results for the on-resonance excitation cases, f=290Hz

sensor	A1	A2	A3	M1	M2	M3	P1	P2	P3
reduction of Φ_w (dB)	49.6	55.3	53.4	53.5	52.8	53.5	49.8	55.3	54.1
reduction of Φ_p (dB)	55.3	52.0	49.8	24.0	59.0	24.0	55.6	52.1	50.1
Voltage (volts)	6.81	6.82	6.81	6.83	6.83	6.83	6.84	6.82	6.81

The wavenumber analysis corresponding to the previous cases in Figure 3 is shown in Figure 4. The LMS value of the velocity transform is plotted over the structural wavenumber, and the acoustic wavenumber is also indicated. Only the wavenumber components less than the acoustic wavenumber, i.e., the supersonic region [15], can radiate into the far-field. The shape of solid line which represents the response due to the disturbance, explain the monopole radiation mode shape for the third mode excitation as shown in Figure 3. A global reduction of $|\tilde{V}|^2$ implies the sufficient control of radiated wave as well as the reduction of radiated power. It is worth to mention that in Figure 4(b) the velocity transform reveals a dip at $k\sin\theta\sin\phi$, right at the angles of the error microphone. The M2 microphone provides the most reduction in the supersonic region, and hence the best sound radiation control can be achieved.

Figure 5 shows the beam displacement distributions corresponding to the previous cases in Figure 3. The solid line indicating the beam response due to the disturbance alone exhibits the third mode response. As accelerometers used as error sensors shown in Figure 5(a), where the accelerometer is located is driven to zero displacement. One can see that the beam response is globally reduced. As shown in Figure 5(b), microphones are used as error sensors. The residual beam response becomes a distorted second mode response. This explains the radiation directivity pattern seen in Figure 3(b). For the use of PVDF sensors, as shown in Figure 3(c). The beam response is also globally reduced. It is interesting to note that the residual response near the PVDF film maintains a constant slope, because the PVDF sensor measures the slope difference between the two edges of PVDF film, and LMS feedforward control algorithm tends to minimize the slope.

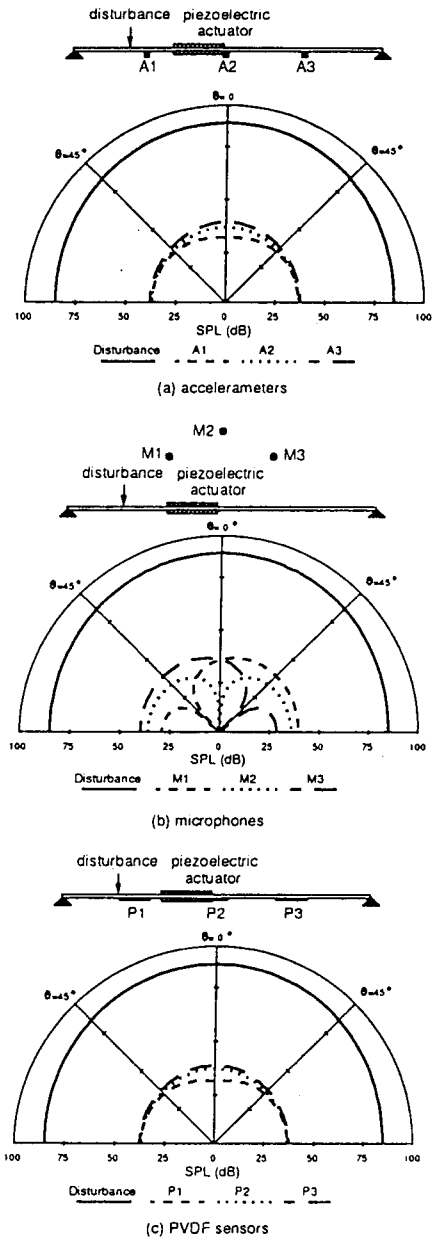

Fig.3 Radiation Directivity Pattern for On-Resonance Case, f=290Hz

3.2 Off-resonance case

For off-resonance excitation f=400Hz, i.e., between the third and fourth resonance modes, Figure 6, 7 and 8 respectively show the radiation directivity pattern, wavenumber distributions and beam displacement distributions for the comparison of accelerometers, microphones and PVDF film sensors. Table 2 summarizes

the results for off-resonance excitation cases. The negative value of reduction of Φ_w and Φ_p indicates control fails. Similar characteristics can be observed as discussed for on-resonance excitation cases. In particular, only little control can be achieved due to the improper location of actuators and sensors. Therefore, it is required to optimize the placement of piezoelectric actuators and PVDF sensors; however, it is out of the content of the paper. The optimization problem of the location of actuators and sensors is currently under investigated in NPPI.

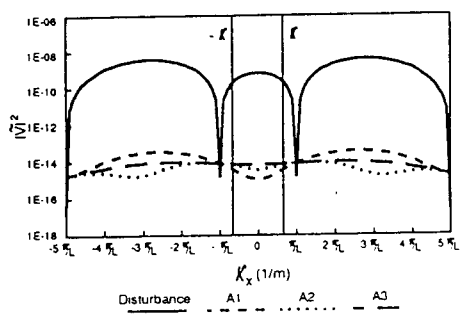

(a) accelerameters

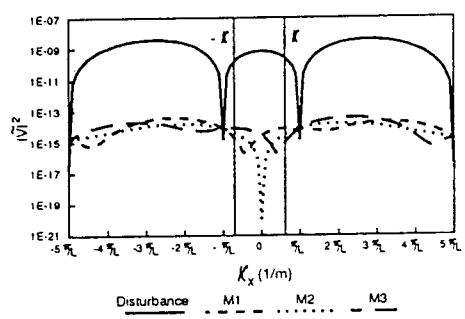

(b) microphones

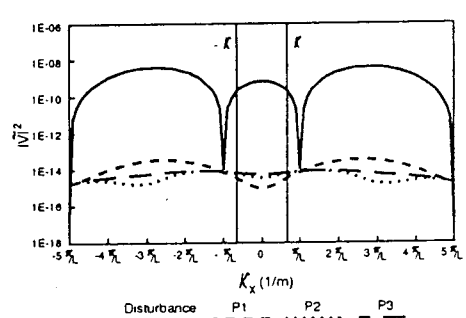

(c) PVDF sensors

Fig.4 Wavenumber Distributions for On-Resonance Case, f=290 Hz

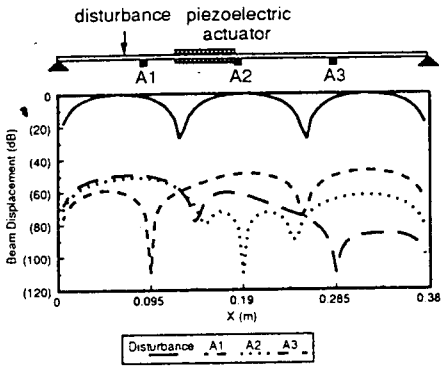

(a) accelerameters

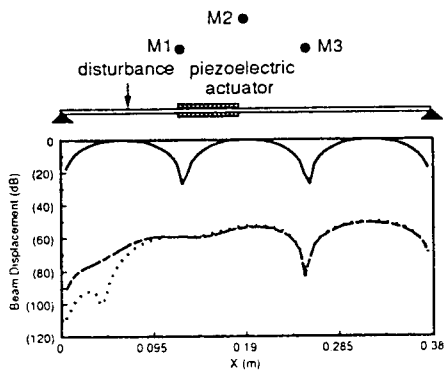

(b) microphones

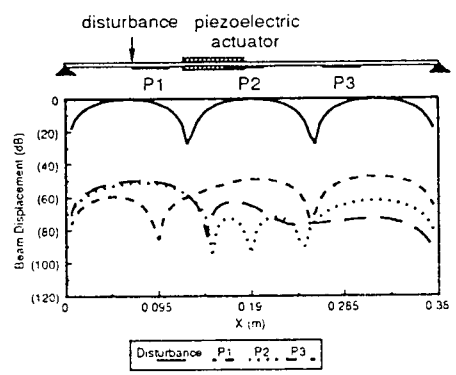

(c) PVDF sensors

Fig.5 Displacement Distribution for On-Resonance Case, f=290Hz

Table 2 Results for the off-resonance excitaiton cases, f=400Hz

sensor	A1	A2	A3	M1	M2	M3	P1	P2	P3
reduction of Φ_w (dB)	-42.2	-1.6	2.9	0.4	-10.7	0.4	-8.0	1.9	2.8
reduction of Φ_p (dB)	-35.4	1.1	1.0	1.2	-4.2	1.2	-3.7	1.1	1.0
Voltage (volt)	-506.6	4.4	2.8	0.26	16.0	0.26	-6.7	4.2	3.2

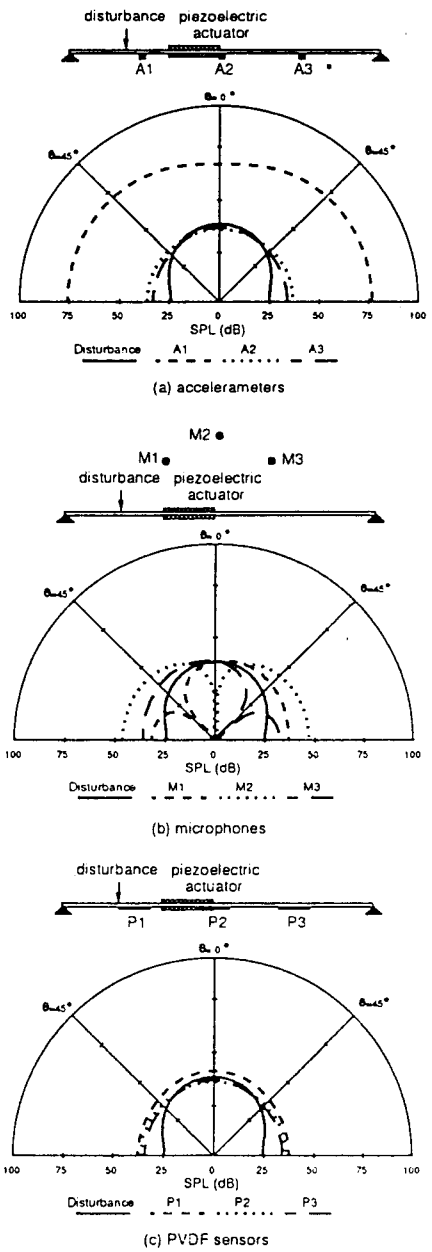

Fig.6 Radiation Directivity Pattern for Off-Resonance Case, f=400Hz

CONCLUSIONS

This work analytically evaluates the performance of accelerometers, microphones and PVDF sensors in ASAC. A simply-supported beam mounted with an infinite rigid baffle subjected to a harmonic point force is considered as the plant. The sound radiation through the beam is actively controlled by applying a control force, i.e., the piezoelectreic actuator, directly to the radiated structure in conjunction with the use of LMS feedforward control algorithm. Different forms of sensors are applied. Results show that sound radiation control can be achieved, if the proper actuators and sensors are selected. Particularly, microphones perform better sound radiation control than accelerometers and PVDF sensors, because microphones can directly measure the acoustic field, while accelerometers and PVDF sensors can only measure the vibrating field. The near-field structural sensors, such as accelerometers and PVDF sensors, have the advantages of easy implementation over the far-field microphones sensors. In particular, the PVDF film, which is a distributed form of sensor, is more practical than the accelerometer or microphone because of its low cost and light weight.

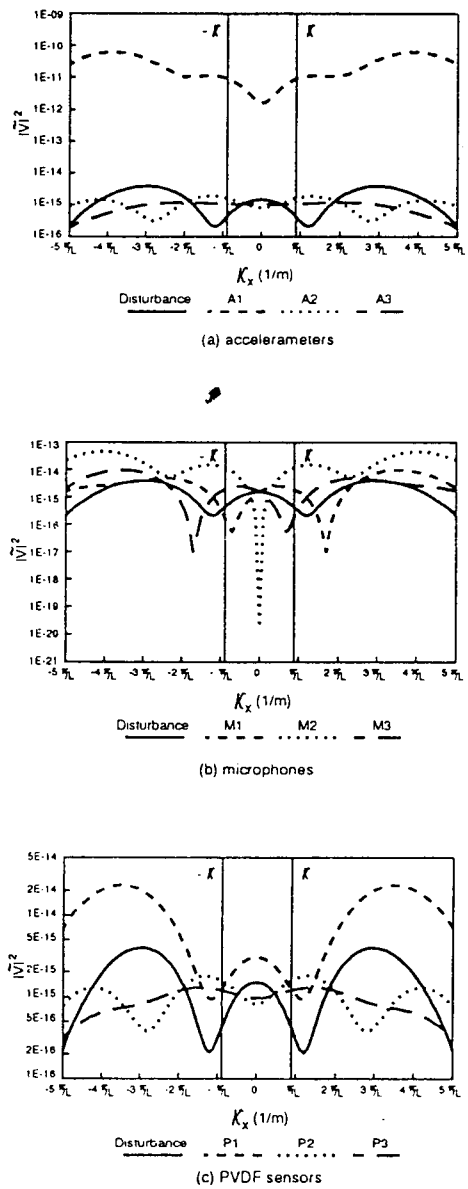

Fig.7 Wavenumber Distribution for Off-Resonance Case, f=400Hz

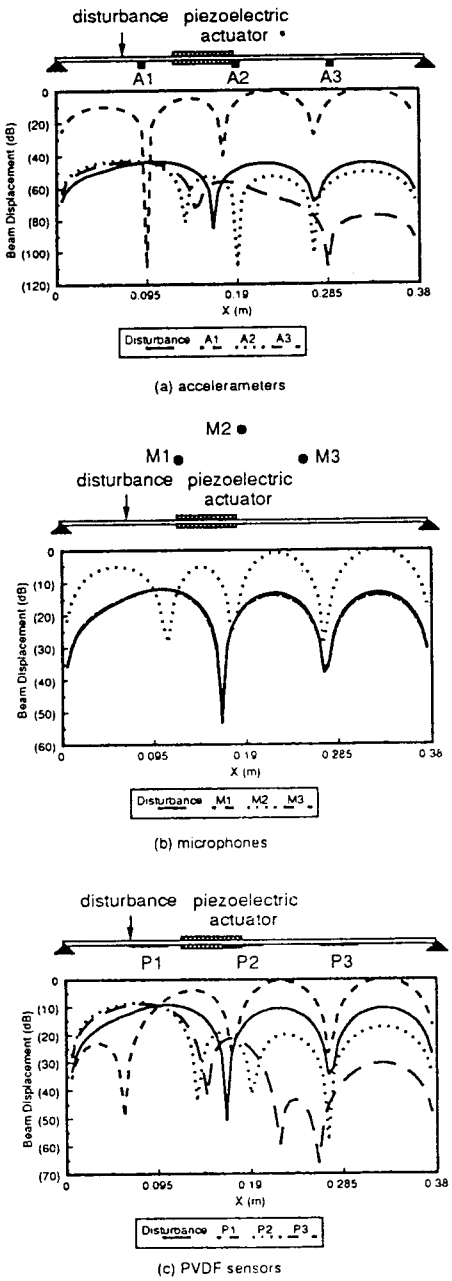

Fig.8 Displacement Distribution for Off-Resonance Case, f=400Hz

ACKNOWLEDGEMENTS

The author gratefully acknowledges the support of the work by National Science Council, Republic of China, under grant NSC82-0410-E-020-001.

REFERENCES

1. Lester, H. C. and Fuller, C. R. "Active Control of Propeller Induced Noise Fields Inside a Flexible Cylinder," AIAA Journal, Vol. 28, No. 8, pp. 1374-1380 (1990).
2. Elliott, S. J., Stoheres, I. M. and Nelson, P. A., "A Multiple Error LMS Algorithm and its Application to the Active Control of Sound and Vibration," IEEE Transaction on Acoustics, Speech and Signal Processing, Vol. ASSP-35, No. 10, pp. 1423-1434 (1987).
3. Burdisso, R. A. and Fuller, C. R., "Theory of Feedforward Control System Eigenproperties," Journal of Sound and Vibration, Vol. 153, No. 3, pp. 437-452 (1992).
4. Lueg, "Process of Silencing Sound Oscillator," U.S. Patent No. 2,043,416 (1936).
5. Deffayet, C. and Nelson, P. A., "Active Control of Low Frequency Harmonic Sound Radiated by a Finite Panel," Journal of Acoustical Society of America, Vol. 84, No. 6, pp. 2192-2199 (1988).
6. Nelson, P. A., Curtis, A. R. D., Elliott, S. J. and Bullmore, A. J., "The Active Minimization of Harmonic Enclosed Sound Fields, Part I: Theory," Journal of Sound and Vibration, Vol. 117, No. 1, pp. 1-13 (1987).
7. Jones, J. D. and Fuller, C. R., "Active Control of Sound Fields in Elastic Cylinders by Multiple Forces," AIAA Journal, Vol. 27, No. 7, pp. 845-852 (1989).
8. Meirovitch, L. and Thangjitham, S., "Control of Sonud Radiation Pressure," Journal of Vibration and Acoustics, Vol. 112, No. 2, pp. 237-244 (1990).
9. Dimitriadis, E. K., Fuller, C. R., and Rogers, C. A., "Piezoelectric Actuators for Distributed Vibration Excitation of Thin Plates," Journal of Vibration and Acoustics, Vol. 113, pp. 100-107 (1991).
10. Wang, B. T., Dimitriadis, E. K. and Fuller, C. R., "Active Control of Structurally Radiated Noise Using Multiple Piezoelectric Actuators," AIAA Journal, Vol. 29, No. 11, pp. 1802-1809 (1991).
11. Clark, R. L. and Fuller, C. R., "Control of Sound Radiation with Adaptive Structures," Journal of Intelligent Material System and Structures, Vol. 2, No. 3, pp. 431-452 (1991).
12. Clark, R. L. and Fuller, C. R. "A Model Reference Approach for Implementing Active Structural Acoustic Control," Journal of Acoustical Society of America, Vol. 92, No. 3, pp. 1534-1544 (1992).
13. Wang, B. T. and Rogers, C. A., "Modeling of Finite-Length Spatially Distributed Induced Strain Actuators for Laminate Beams and Plates," Journal of Intelligent Material System and Structures, Vol. 2, No. 1, pp. 38-58 (1991).

14. Lee, C. K. and Moon, F. C., "Modal Sensors/Actuators," Journal of Applied Mechanics, Vol. 57, No. 2, pp. 434-441 (1990).

15. Fahy, F., "Sound and Structural Vibration," Academic, Orlando, Florida, U.S.A. (1985).

16. Wallace, C. E., "Radiation Resistance of a Baffled Beam," Journal of Acoustical Society of America, Vol. 51, No. 3, pp. 936-945 (1972).

17. Wang, B. T., "A Dynamic Simulation of Hybrid Active and Passive Control of Structural Vibration," NSC Report, NSC81-0401-E-020-501, R.O.C. (1992).

18. Piezo Systems, Inc., Product Catalog, Cambridge, Massachusetts, U.S.A. (1990).

19. Pennwalt Corporation, Piezo Film Sensor Applictions Notes, Valley Forge, Pennsylvania, U.S.A. (1990).

加速度計、麥克風和壓電薄膜在主動結構噪音控制之評估

王柏村

中華民國　台灣省　屏東縣

國立屏東技術學院機械工程技術系

摘　要

本文理論性探討加速度計、麥克風、壓電薄膜在主動結構噪音控制之效果，一諧振動點力作用於一無限長剛體屏障之簡支樑爲干擾源，壓電驅動器黏貼於樑表面則作爲控制源，以減小樑之聲音輻射，爲達成聲音輻射控制，分別使用幾種不同的感應器，採用一最佳化程序，以求得輸入壓電驅動器之最佳電壓，使得成本函數最小化，此成本函數則爲誤差感應器信號之最小平方值。結果顯示，如果適當地選擇驅動器及感應器可以減小樑之聲音輻射，此外，麥克風比加速度計或壓電薄膜在聲音輻射控制更有效果，但是由於壓電薄膜輕巧且低成本使得比加速度計或麥克風更有實用價值。

關鍵詞：加速度計、麥克風、壓電薄膜，聲音輻射，控制

(Manuscript received Dec. 27, 1993,
Accepted for publication Jun. 20, 1994.)